Pollution 2022, 8(4): 1308-1324
DOI: 10.22059/POLL.2022.342339.1458

RESEARCH PAPER

Green Synthesis of ZSM-5@rGO Composite for Adsorption of Methylene Blue from Aqueous Solution

Xuan Nui Pham* and Hoa Thi Nguyen

Department of Chemical Engineering, Hanoi University of Mining and Geology, 18 Vien Street, Duc Thang Ward, Bac Tu Liem, Hanoi, Vietnam.

Received: 01.05.2022, Revised: 19.06.2022, Accepted: 21.07.2022

Abstract
A green approach was employed to fabricate ZSM-5 zeolite from expanded perlite and reduced graphene oxide (rGO) in the presence of the synthesized ZSM-5 zeolite to produce ZSM-5@rGO composite by one-step synthesis process via hydrothermal treatment. ZSM-5@rGO composites were characterized by various techniques such as scanning electron microscopy (SEM), X-ray diffraction (XRD), Fourier transform infrared (FT-IR) spectroscopy, Raman spectroscopy, and N_2 desorption–adsorption. The results showed that ZSM-5@rGO composite have a large surface area, uniform distribution and orderly crystal form. Moreover, the synthesized composites were evaluated as an adsorbent for removing cationic dye, methylene blue (MB), from an aqueous solution. The influence of factors on the adsorption, such as adsorption time, adsorbent dosage, initial dye concentration, and pH of solution, were investigated. The results of isothermal adsorption showed that the adsorption process was fit for both Langmuir and Freundlich models, and the highest adsorption capacity of ZSM-5@rGO composite for MB dye was 95.87 mg/g at environment temperature (30 °C). In addition, the study of adsorption kinetics indicated that the adsorption was consistent with the pseudo-second-order kinetic model with correlation coefficients of 0.9962. From these results, it can be confirmed that ZSM-5@rGO composite uses silicoaluminate as economical starting material with relatively high adsorption capacity and removal efficiency, which is a promising application for treating wastewater on a large scale.

Keywords: Reduced graphene oxide, expanded perlite, ZSM-5, ZSM-5@rGO, MB

INTRODUCTION

The elimination of dyes from textile industry wastewater plays a vital role in terms of human health and environmental protection due to their solubility and stability in water at any concentrations (Bagane et al., 2000; Imamura et al., 2002). Therefore, with the widespread occurrence of dyes in many industries, the dyes removal process has received great attention from researchers. Until now, various techniques have been applied to remove dyes including physical (Uddin et al., 2009), chemical (Sismanoglu et al., 2010), and biological methods (Gök et al., 2010), of which adsorption has received intensive study thanks to its low investment cost, simple operation as well as low power consumption. Besides, this process also produces odorless water and could reduce water consumption in industrial waste disposal.

Activated carbon is a common adsorbent for the removal of pollutants in wastewater due to its large surface area and high capacity for adsorption. However, the low selectivity and regeneration, and the high cost of production have limited its application (Dai, 1998). Meanwhile, zeolite derived from cheap natural minerals is often used as an adsorbent to

* Corresponding author Email: phamxuannui@humg.edu.vn

effectively remove ammonium (Taddeo et al., 2017), phenol (Liu et al., 2020), heavy metal ions (Belova et al., 2019), and gases (Hauchhum et al., 2014). Synthetic zeolites generally have a more uniform pore structure and higher adsorption capacity than natural zeolites (Król, 2020). The synthesis of zeolites and its functionalization with a low-cost and high efficiency for wastewater treatment has attracted extensive attention. Typically, ZSM-5 is synthesized mainly from organic compounds of silicon such as TEOS (tetraethylorthosilicate), TMOS (tetramethyl orthosilicate), TPOS (tetrapropoxysilane) (Navrotsky et al., 1994; Chen, 1996). However, these compounds are expensive and pose threats to the environment due to their toxicity. Over the past decades, ZSM-5 synthesis processes have been optimized to reduce manufacturing costs and environmental impact by using natural clay minerals such as clay (Feng et al., 2015), and perlite (Filho et al., 2018) and fly ash (Liu et al., 2020),... Of these, perlite is known to be a glassy rock composed mainly of aluminum silicate and containing 2–5% combined water, which allows it to be expanded approximately 20 times that of pure perlite by heating. Many researches have shown that zeolite can be prepared from a cheap precursor such as expanded perlite. Faghihian et al. (2003) reported the preparation of Na-Pc zeolite from perlite by the hydrothermal method and its ability to remove cyanide from liquid wastes. Some successful studies have been previously reported using expanded perlite for the synthesis of zeolites (Corregidor et al., 2014; Da Silva Filho et al. 2018; Magdalena et al. 2014). Xuan et al. (2020) reported the synthesis of O-g-C_3N_4/HZSM-5 composite from expanded perlite as a photocatalyst for the degradation of RR-195 under sunlight.

Graphene-based materials have become widely available for environmental treatment due to their large surface area and presence of functional groups (Yang et al., 2013). However, also due to their hydrophilic nature, GO sheets are difficult to separate, which may cause secondary contamination of aqueous solution. Therefore, the incomplete reduction may produce unreduced oxygen-containing functional groups and defects for reduced-graphene oxide (rGO), leading to good adsorption capacity (Yushan et al., 2014; Li et al., 2011; Vu et al. 2020).

Some studies have recently found that the combination of rGO with an inorganic material can create a good composite for the removal of pollutants in the aquatic environment (Li et al., 2011; Liu et al. 2014). Adsorption composites containing rGO and zeolite are commonly used, according to previous research (Khatamian et al., 2017; Kim et al. 2018; Choudhury et al., 2021). Several methods for synthesis of zeolite–rGO composites have been developed, of which the hydrothermal method is the most widely used (Li et al. 2012; Khatamian et al., 2015). Ni-rGO-zeolite nanocomposite was used as effective heterogeneous catalyst for the one-step synthesis of triazoles in water (Prasun et al. 2021). rGO-zeolite composite showed that high efficiency in purification of aged oil from transformer machines (Tan et al. 2022).

In this study, we used a green process for the synthesis of ZSM-5 zeolite from expanded perlite as the starting material under different crystallization time conditions. Reduced-Graphene oxide in the presence of the synthesized ZSM-5 to create the unique structure of ZSM-5@rGO composite with Van der Waals forces. The synthesized composites were investigated for the removal of cationic dye, MB, from aqueous solution.

EXPERIMENTAL

Chemicals

Perlite mineral (Phu Yen, Vietnam), which contains 68.51% SiO_2, 14.54% Al_2O_3. Graphite (99%), sodium silicate (Na_2SiO_3, 99%), tetrapropylammonium hydroxide (TPAOH, 1 M in H_2O), sulfuric acid (H_2SO_4, 98%), potassium permanganate ($KMnO_4$, 99%), hydrogen peroxide (H_2O_2, 30%), sodium nitrate ($NaNO_3$, 98%), sodium hydroxide (NaOH, 99%) are from Sigma–Aldrich Company and used without any purification.

Synthesis of ZSM-5 zeolite

2.0 g of the raw perlite was added to 100 mL of distilled water. The mixture was stirred continuously by a paddle for 24 h. Then, the mixture was then settled for one day, and decanted the middle part of the mixture. The pure perlite was then filtered, dried, and calcined at 900 °C for 3 h before being collected as a starting material for the synthesis of ZSM-5 zeolite.

A hydrothermal crystallization method was used to synthesize ZSM-5. For typical procedure, the exact amounts of expanded perlite and NaOH were dissolved in distilled water at 80 °C. After 30 min, TPAOH was added to the homogenous solution and stirred for 60 min. The mixture was adjusted to a pH of 10 using H_2SO_4. The composition of the mixture included SiO_2/Al_2O_3=50, H_2O/SiO_2=45, $TPAOH/SiO_2$=0.02, Na_2O/SiO_2=0.26 (molar ratio). The gel was kept at room temperature for 24 h and then it was placed in a Teflon-lined autoclave at 180 °C for 24, 48, and 72 h. After the hydrothermal process, the solid was washed with distilled water and dried at 110 °C overnight. Finally, ZSM-5 zeolite was obtained after calcining the product at 550 °C for 6 h. ZSM-5 samples were donated as Z–24, Z–48, and Z–72, respectively.

Synthesis of reduced–graphene oxide coated ZSM–5 composite (ZSM-5@rGO)

Firstly, GO was synthesized from graphite powder using modifying Hummer's method (Hummers et al. 1958; Vuong et al. 2020). In a typical synthesis, 1 g of graphite powder was mixed with 23 mL of 98 % H_2SO_4 and 0.5 g of $NaNO_3$. The mixture was stirred for 30 minutes in an ice bath at 0 °C. Next, 3 g of $KMnO_4$ was carefully added to the suspension while maintaining its temperature below 20 °C. After the solution was stirred for 30 min, 46 mL of distilled water was slowly added. After that, 10 mL of 30% H_2O_2 was slowly dropped and stirred until the color of the mixture changed light brown. This mixture was filtered and washed with 0.1 M HCl and distilled water until the pH was close to 7. Finally, the samples GO was dried at 80 °C for 24 h to obtain GO powder. The reduction of GO to rGO was performed by heating the mixture to 80 °C and adding V mL of 1 M $NaBH_4$ solution.

Next, the exact amounts of expanded perlite and NaOH were dissolved in distilled water at 80 °C. TPAOH, rGO was added after 30 min of homogeneous suspension and continuously stirred for 60 min. The mixture was adjusted to a pH of 10 using H_2SO_4. The composition of the mixture included SiO_2/Al_2O_3=50, H_2O/SiO_2=45, $TPAOH/SiO_2$=0.02, Na_2O/SiO_2=0.26 (molar ratio), and rGO/ZSM-5=2:1, 1:1 and 1:2 (weight ratio), respectively. The suspension was aged for 24 h at room temperature, and transferred into a Teflon-lined stainless steel autoclave and kept at 180 °C for 24 h. Finally, the solid was washed, dried at 110 °C overlight, and obtained the ZSM-5@ rGO composites (denoted as rGZ-2:1; rGZ-1:1, and rGZ-1:2).

Characterization

The X-ray diffraction (XRD) patterns were performed with CuKa radiation (λ=1,5406 A°) on a D8 ADVANCE, Bruker with scanning rate of 3°/min from 2 theta 5 to 80°. The morphologies of the synthesized samples were investigated using scanning electron microscope (SEM) JSM-6340LV at an operating voltage of 15. The FT-IR spectra of the materials were performed on FTIR Affinity–1s, Shimadzu spectrophotometer, in the range of 400–4000 cm^{-1}. The Raman spectra were collected on Nanofinder 30 Confocal Raman using an excitation wavelength at 532 nm. BET surface area and the porosity characteristics were determined by nitrogen adsorption/ desorption isotherm using Chem BET–3030 porosimetry at liquid nitrogen temperature (77 K).

Methylene blue dye adsorption

The MB adsorption process was performed at the desired dye concentrations, adsorbent dosage, adsorption time and pH value in a flask containing 50 mL of test solution under continuous stirring at environment temperature (30 °C). At a specific time, the dye solution was decanted and centrifugated and then the equilibrium MB concentration was measured by

UV−Vis absorption spectroscopy at the wavelength of 664 nm. The MB adsorption efficiency, R (%), adsorption capacity at time t, Q_t (mg/g), and at equilibrium, Q_e (mg/g) were determined using below equations:

$$R(\%) = \frac{(C_o - C_t)}{C_o} 100 \quad (1)$$

$$Q_t\,(\text{mg/g}) = \frac{(C_o - C_t)V}{m} \quad (2)$$

$$Q_e\,(\text{mg/g}) = \frac{(C_o - C_e)V}{m} \quad (3)$$

where C_o, C_t and C_e are respectively initial concentration, concentration at time t and at equilibrium time of MB solution (mg/L); V is volume of MB solution (L); m is mass of adsorbent (g).

Point of zero charge (PZC) determination method

A salt addition method was used to determine the point of zero charge of the ZSM-5@rGO composite (Jorge et al. 2008). Briefly, 0.05g sample was added to 40 mL of 0.1M $NaNO_3$ in 100-mL glass Erlenmeyer flasks. The pH was adjusted as needed with 0.1 M HNO_3 and 0.1 M NaOH to achieve the desired pH range of 2 to 12. The pH values of the supernatant were denoted as pH_i. The samples were shaken for 24 hours at 200 rpm in a revolving water bath to reach equilibrium. After 24h, the pH values of the supernatant were measured and denoted as pH_f. The difference between the initial and final pH values ($\Delta pH = pH_i - pH_f$) against the initial pH was plotted. The pH value where ΔpH was zero was taken as the *pzc*.

RESULTS AND DISCUSSION

Characterization of samples

The XRD patterns were performed to determine the phase composition and calculate the crystallinity percentage of the synthesized zeolite samples. The phase structure of ZSM−5 zeolite was determined by 2θ peaks from 5° to 45°. The crystallinity was calculated by comparing the total area of all peaks from 22° to 25° with a reference ZSM-5 (Si/Al=67, denoted as ZSM−5/R) (Filho et al., 2018). XRD pattern of Z−24, Z−48, Z−72, and ZSM−5/R samples are presented in Fig. 1a. It is clear that the as-synthesized ZSM-5 samples have clear peaks at 2θ=7.9°, 8.8°, 23°, 23.9°, 24.4° attributed to MFI topological structure of ZSM-5 zeolite (Filho et al., 2018).

Herein, we have determined the crystallinity of the synthesized ZSM-5 samples by comparison with the reference ZSM-5 zeolite sample, which had very good crystallinity. The calculation formula is shown below:

$$\text{crystallinity (\%)} = \frac{\text{2-theta peak area from 22.5 to 25.0° of product}}{\text{2-theta peak area from 22.5 to 25.0° of reference sample}} \quad (4)$$

The results from Table 1 show that all of the synthesized ZSM-5 zeolites had high crystallinity, in which the Z-48 sample with the highest crystallinity being 88%. Also, from the X-ray diffraction peak intensity observed in the area of 2θ from 7.5 to 8.2° declines with extending the reaction time. The intensity of these peaks changes indicating that the growth of the crystal plane has transferred after an increase in reaction time. However, this increase was not significant, therefore, the crystallization time of 24 h was chosen to synthesize ZSM-5 zeolite.

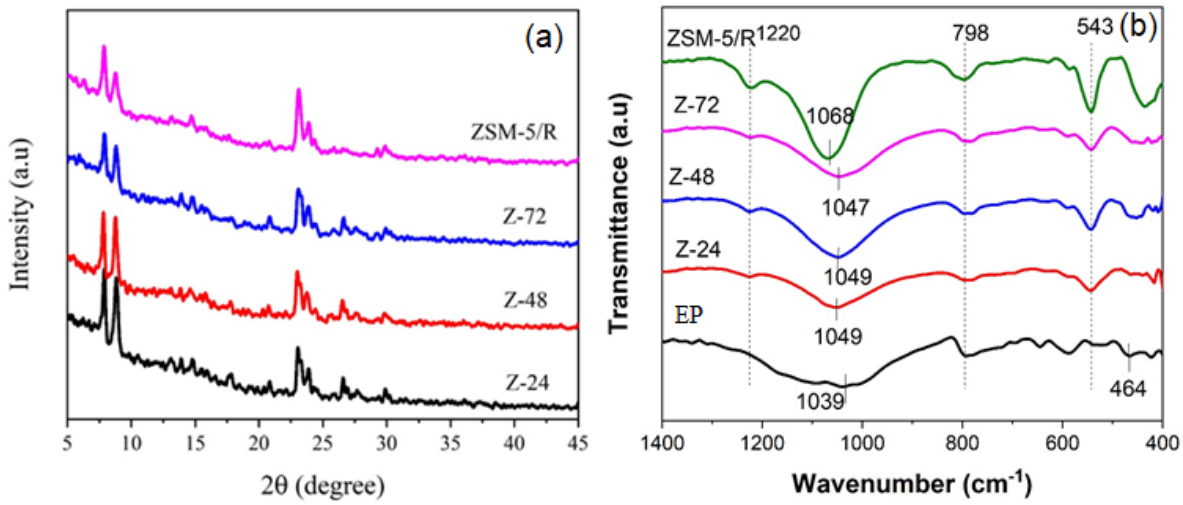

Fig. 1. (**a**) XRD patterns of Z–24, Z–48, Z–72, and ZSM–5/R samples, (**b**) FT–IR spectra of EP, Z–24, Z–48, Z–72, and ZSM–5/R samples

Table 1. Crystallization of the synthesized samples

Sample	ZSM–5/R	Z–24	Z–48	Z–72
Crystallinity (%)	100	87	88	82

Fig. 1b shows the FT–IR spectra of expanded perlite, Z–24, Z–48, Z–72 and referenced zeolite. The infrared band revealed the presence of expanded perlite at 1039 cm^{-1} corresponds to the Si–O–Si group vibration in the structural siloxane framework because of its amorphous silica content. The region band at around 792 cm^{-1} is due to Si-O-Si symmetric stretching in perlite samples, additional peak at 464 cm^{-1} is attributed to bending modes of Si-O-Si and O-Si-O (Abalos et al., 2003).

For the synthesized ZSM-5, the absorption peaks at 1220 cm^{-1} and 543 cm^{-1} indicating the distinction between ZSM–5 and other kinds of zeolite. The asymmetric stretching vibration of O-T-O (where T is Al or Si) at the absorption peak of 1220 cm^{-1} indicates the appearance of four chains of five-membered rings arranged around a two-fold screw axis presenting the structure of ZSM-5 (Wang et al., 2013). The strong absorption peak at 543 cm^{-1} was characteristic of the double five-membered ring in the structure of ZSM-5 zeolite. The region at around 1049 cm^{-1} corresponds to the Si-O-T linkages asymmetric stretching vibration (Fan et al., 1995). The absorption peak around 798 cm^{-1} corresponded to the symmetric vibration from inter-tetrahedral of TO_4, while the absorption peak at 436 cm^{-1} was attributed to the T–O bending vibrations of SiO_4 and AlO_4 (Zhang et al., 1995). The peaks at 543 and 436 cm^{-1} were characteristic of the crystalline structure of ZSM-5, and the ratio of the adsorption band intensities at 543 cm^{-1} and 450 cm^{-1} was considered a reliable index for evaluating the crystallinity of the synthesized zeolite samples. From the obtained results of the as-synthesized Z–24, Z–48, and Z–72, the I_{543}/I_{436} were 0.78, 0.79, and 0.74, respectively, while the ZSM–5/R suggested a value of 0.8 (Filho et al., 2018). This confirms that the fabricated ZSM–5 zeolite samples have high crystallinity.

The morphologies of expanded perlite and the Z–24 are shown in Fig. 2. Expanded perlite had a crystal-like porous, high surface pores, and rough surface (Fig. 2a). In Z–24 sample, the crystal grains grew to the cubic form of the ZSM-5 crystals and a typical hexagonal-shaped MFI crystal structure was clearly observed (Fig. 2b). However, some smaller crystalline grains or even amorphous form were observed, which may be hindered by the parent materials.

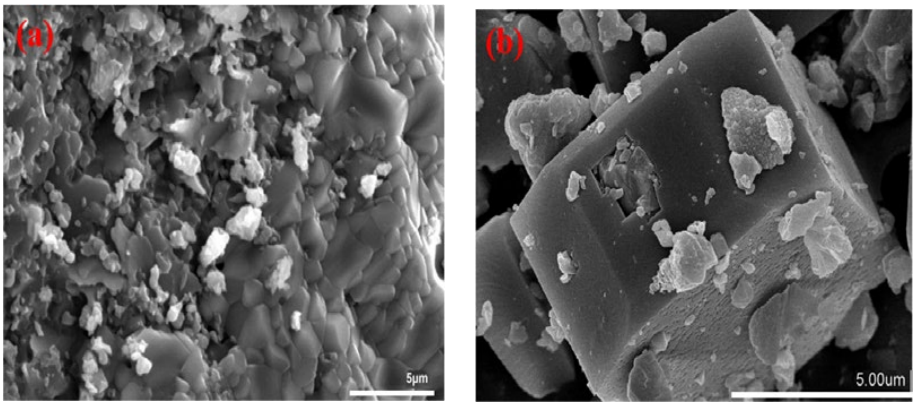

Fig. 2. SEM images of (**a**) expanded perlite (EP), (**b**) Z–24 sample

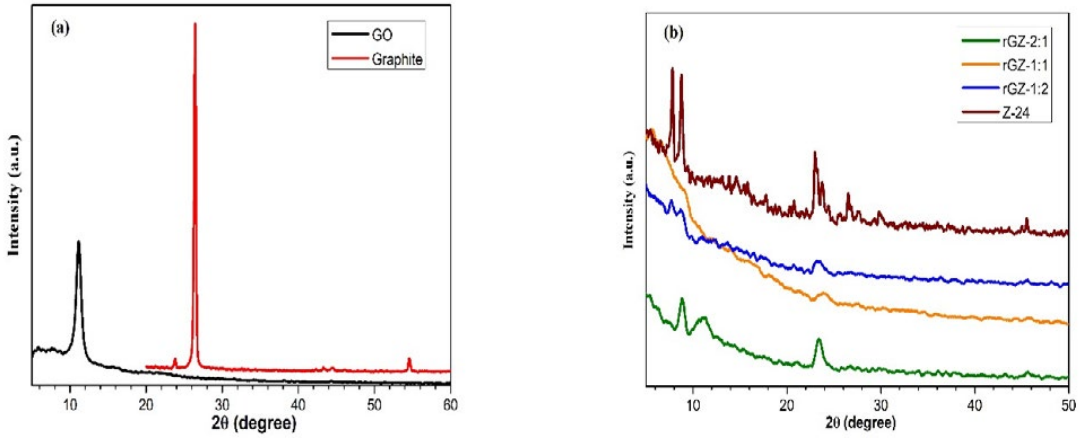

Fig. 3. XRD patterns of (**a**) graphite and GO (**b**) Z–24, and rGZ–1:2, rGZ–1:1 and rGZ–2:1 composites

Fig. 3a shows the XRD results of the graphite and the fabricated graphene oxide. The peak at 2θ=26.5° corresponds to the graphite structure. After treatment in the presence of strong acid (H_2SO_4) and oxidation agents ($KMnO_4$ and $NaNO_3$), this peak was shifted to 2θ=11°, characterizing graphene oxide structure (Ramesha et al., 2011). The insertion between the graphite layers by oxygen-containing functional groups such as epoxy (–O–), hydroxyl (–OH), carbonyl (–C=O), carboxylic (–COOH), resulting in an expansion in the distance between the layers so that the peak at 25.5° disappears and was replaced by the peak at 11° (Gao, 2015). Fig. 3b shows the XRD pattern of ZSM–5 and ZSM–5@rGO composites. For ZSM–5@rGO composites, the presence of the reduced graphene oxide was confirmed by peak at 2θ=23.4°. The relatively weak diffraction peaks have also appeared at 2θ=7.9°, 8.8°, which are attributed to ZSM–5 zeolite crystals. Meanwhile, the characteristic peaks for ZSM-5 at 23.9°, 24.4° disappears. This may be due to the ZSM-5 crystals being interspersed into the layers and cavities of rGO, thus, no peak appeared on the XRD patterns. The results of FT-IR, and SEM demonstrated the presence of ZSM-5 in composite materials.

The structural change of GO reduction to rGO was analyzed by Raman spectroscopy. The typical peaks of GO and ZSM-5@rGO composite were detected as in Fig. 4a. The G band at 1593 cm^{-1} corresponded to sp^2 hybridization of carbon atoms. The D band at 1337 cm^{-1} was attributed to the defect structure of sp^3 hybridization of carbon atoms. The I_D/I_G value (intensity ratio between D and G band) indicates the ratio between sp^3 and sp^2 hybridization of some carbon atoms and characteristic of the extent of disorder of the graphite material. The lower the

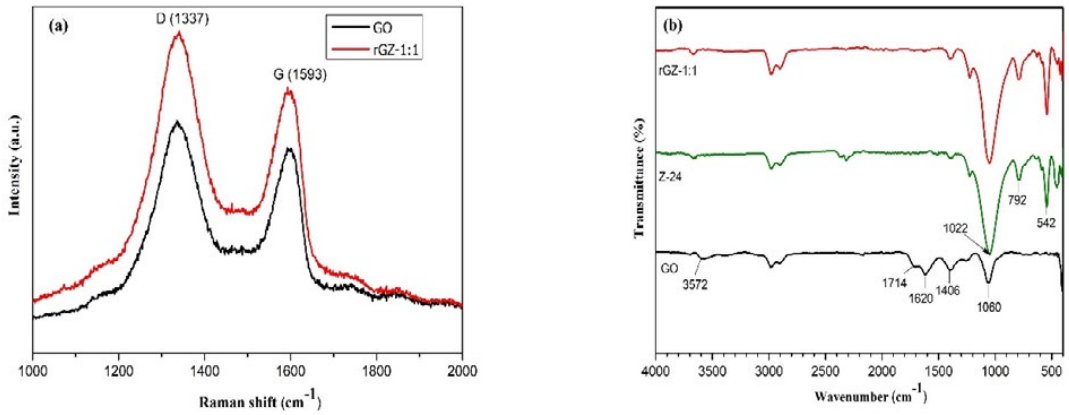

Fig. 4. (**a**) Raman spectra of GO and rGZ−1:1 composite, (**b**) FT−IR spectra of GO, Z−24, and rGZ−1:1 composite

I_D/I_G ratio, the better the reduction of GO to rGO (Hernandez et al., 2013; Mei et al. 2015). GO has a lower ratio than RGZ-1:1 composite (1.1<1.17). It can be explained as GO was reduced and losing its oxygen-containing functional groups, forming rGO and lowered sp^2 carbon hybridization. This result was also consistent with previous studies (Khatamian et al., 2015).

The FT-IR spectra of GO, ZSM-5 and rGZ-1:1 composite are illustrated in Fig. 4b. In GO spectrum, the peaks at 1714 cm^{-1} and1620 cm^{-1} corresponded to the stretching vibrations of C=O, and C=C. The peak at around 3572 cm^{-1} related to the stretching vibration of hydroxyl (-OH) groups present in GO. Furthermore, the peaks that appeared at 1406 cm^{-1} and 1060 cm^{-1} were the stretching vibration of C-O groups related to carboxyl and epoxy groups, respectively (Sourav et al., 2016). In rGZ-1:1 composite spectrum, the characteristic absorption bands at 1022, 792, and 542 cm^{-1} were assigned to various vibrations of the TO_4 (where T is Si or Al) tetrahedral unit of ZSM-5 zeolite (Zhang et al., 2010). Besides, no absorption peaks appeared at 1714, 1620 cm^{-1}, which confirmed that GO had been reduced to rGO.

The surface morphology of the rGZ-1:1 composite was analyzed by SEM images (Fig.5). It is evidence that at different ZSM-5@rGO ratios, ZSM-5 zeolite crystals were either attached to the surface or alternated between the graphene layers (Fig. 5b,c,d). After attaching rGO nanosheets, the as-fabricated ZSM-5@rGO revealed that the crystalline grains of ZSM-5 was inserted into the layers of rGO. This self-assembly may be formed by hydrogen bonds and van der Waals forces between zeolite and graphene oxide (Liu et al., 2014).

The textural characteristics of samples were examined from nitrogen adsorption-desorption isotherms and are shown in Fig. 6. As shown in Fig. 6A(a), N_2 adsorption-desorption for expanded perlite is classified as II type, indicating that perlite contains non-porous solids or macroporous greater than 50 nm and no microporous solids exist in the structure of type I.

According to the IUPAC classification, the hysteresis curves of Z−24 and rGZ−1:1 were combined both type I and IV (Fig. 6). With the low relative pressure region at P/P_o=0.02 and the H4 hysteresis loop at relative pressure from 0.45 to 1.0 indicated that the presence of both micropores and mesopores in material samples.

The obtained results from Table 2 illustrated that both surface area, pore volume of rGZ−1:1 composite was considerably lower than that of Z−24. This decrease in surface area and pore volume is related to the interaction between oxygen ions on rGO and the negative charge of zeolite in composite, which led to the adhesion of the rGO layers to the surface and pore channels of ZSM−5 (Cadiam et al., 2016; Vuong Hoan et al., 2016). Also, we observed that the pore size distribution of these samples ranges from 2.46 nm to 3.15 nm (Fig. 6B), indicating the presence of mesopores in the samples.

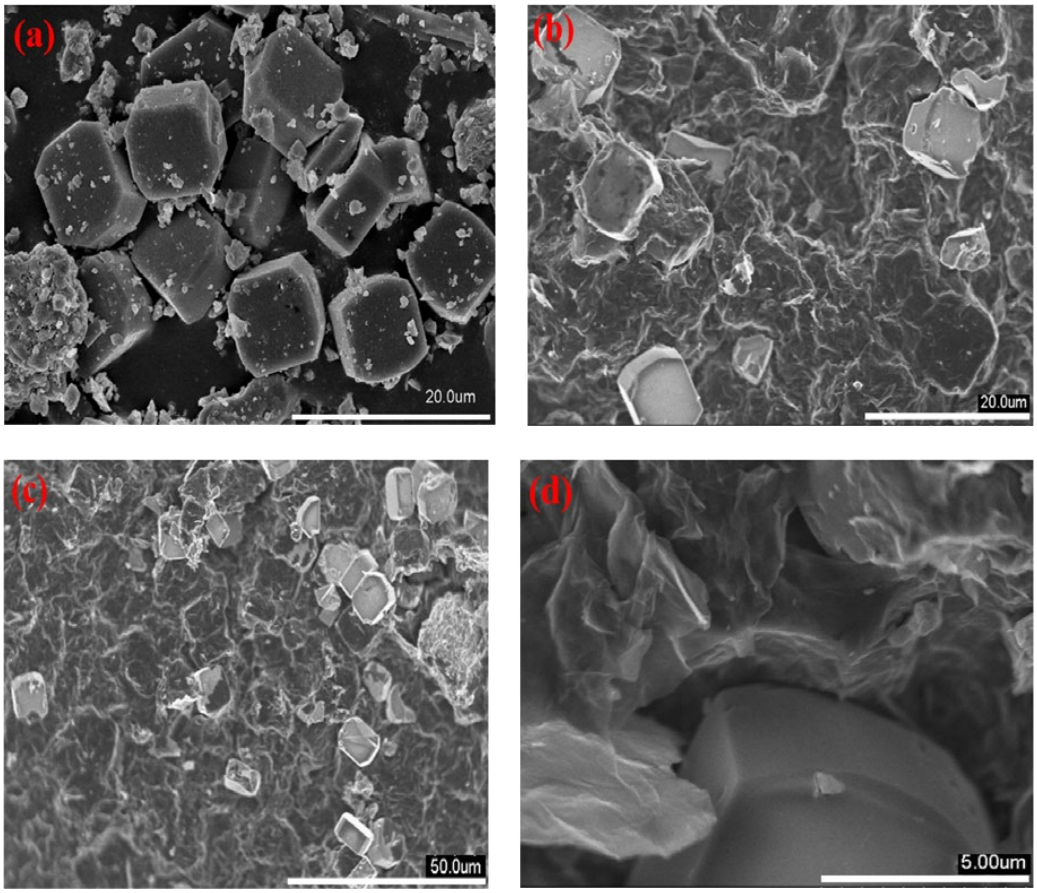

Fig. 5. SEM images of Z−24 (**a**), rGZ−1:1 composite (**b**,**c**,**d**)

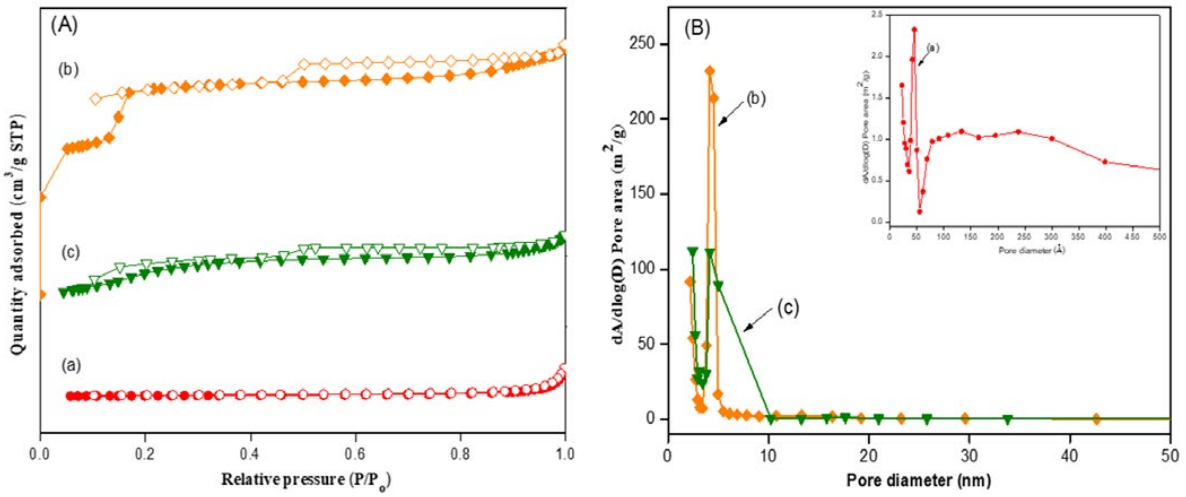

Fig. 6. N_2 adsorption-desorption isotherm (A), and BJH corresponding pore size distribution curve (B) of (**a**) expanded perlite, (**b**) Z−24, and (**c**) rGZ-1:1 composite

The isoelectric point is a vital surface factor that is closely related to material adsorption mechanisms. The experimental result is shown in Fig. 7, the isoelectric point of rGZ-1:1 composite was calculated to be 8.37. The material surface became positively charged due to H^+ ion adsorption in an aqueous solution when the solids were dispersed in water with a pH lower than isoelectric pH. Hence, rGZ-1:1 composite has well adsorption ability with MB dye.

Table 2. Textural properties of synthesized materials

Samples	S_{BET} ($m^2 g^{-1}$)	S_{micro} ($m^2 g^{-1}$)	S_{meso} ($m^2 g^{-1}$)	D_{BJH} (nm)	V_{pore} ($cm^3 g^{-1}$)	
					V_{total}	V_{micro}
Expanded perlite	1.92	0	0	26.39	0.01	0
Z-24	286.04	244.54	41.5	2.46	0.15	0.09
rGZ–1:1	117.47	83.97	33.5	3.15	0.07	0.03

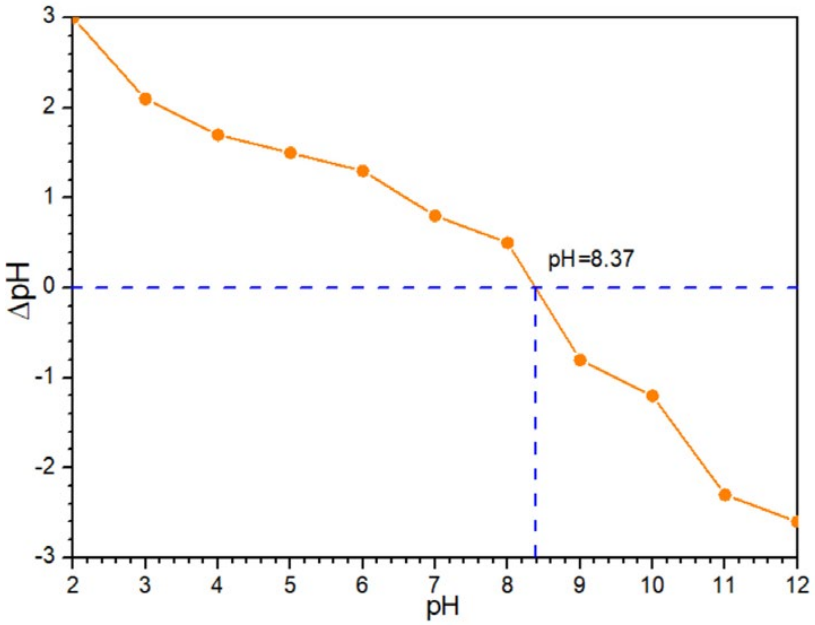

Fig. 7. Point of zero charge for rGZ-1:1 composite

Dye adsorption of rGZ-1:1 composite

Effect of ZSM-5 contents

The composite samples including rGZ–2:1, rGZ–1:1, and rGZ–1:2 were used to investigate the adsorption efficiency. 0.015 g of adsorbent in 50 mL of MB aqueous solution (50 mg/L) for the desired time at 30 °C and pH of 6.2 (pH of MB solution). The results are presented in Fig. 8.

From the obtained results showed that under the same adsorption conditions, after 2 h, rGZ–1:1 had the highest adsorption efficiency of 95.87 %, while rGZ–1:2 and rGZ–2:1 were 79.33 % and 88.82 %, respectively. The effective adsorption of MB dye with rGZ composite was presumably due to aromatic ring π-π interaction of MB molecules with the graphitic framework of rGO in composite samples. In addition, the electrostatic interaction between the negatively charged oxygen functionality groups of the rGO and the positively charged amino groups of MB molecules enhanced MB adsorption on ZSM–5@rGO surface (Chen et al., 2013). ZSM–5 with a high surface area significantly improved MB adsorption efficiency. Moreover, the presence of ZSM–5 prevents of the agglomeration of rGO layer, thereby increasing adsorption of MB dye. rGZ-1:1 was more effective than rGZ-2:1 and rGZ-1:2, as the excess rGO or ZSM-5 could form aggregates that prevented the adsorption rate of MB in ZSM–5@rGO composite.

Effect of adsorption time

The effect of adsorption time was studied with different times ranging from 30 to 180 min,

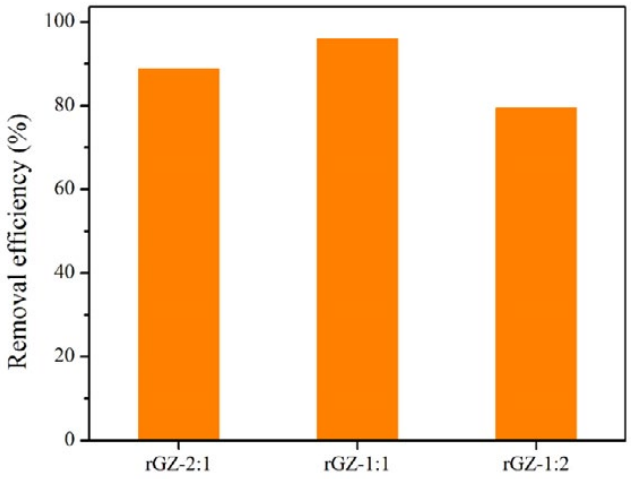

Fig. 8. Dye removal efficiency of each composite rGZ-2:1; rGZ-1:1 and rGZ-1:2
(Reaction conditions: pH 6.2; adsorbent dosage: 0.015 g; initial concentration of MB: 50 mg/L; adsorption time: 2 h; adsorption temperature: 30 °C)

50 mL of initial concentration of MB (50 mg/L), 0.015 of adsorbent at 30 °C, and pH 6.2. The results were illustrated in Fig. 8a. The adsorption capacity increased from 64.53 to 96.07 mg/g with the rise of adsorption time from 10 to 120 min. However, MB removal efficiency remains unchanged with further increasing adsorption time, which was ascribed to saturation of rGZ-1:1 composite. Therefore, 120 min was chosen for further studies.

Effect of adsorbent dosage

The effect of adsorbent dosage on adsorption of MB was investigated by varying amounts of rGZ-1:1 composite with 50 mL of MB (50 mg/L) at adsorption temperature of 30 °C for 120 min and pH 6.2. Fig. 8b showed that when the rGZ-1:1 dosage increased between 0.01 and 0.04 g, the MB removal efficiency increased from 89 to 99%. The adsorption efficiency is enhanced with the rise of adsorbent dosage because of the increase in active sites on surface of composite and thus promote the dye adsorption onto surface sorption sites. With further increase in the adsorbent dosage from 0.02 to 0.04 g, the adsorption efficiency of MB dye was almost unchanged. However, adsorption capacity declined from 95.87 to 37.19 mg/g with that increased the amounts of adsorbent. Therefore, to obtain high adsorption capacity and adsorption efficiency, 0.015 g of rGZ-1:1 was chosen as the optimum dosage.

Effect of pH

The change in pH of solution has a strong influence the adsorption of cationic dyes because the positively charged ions (protons) themselves are in strong competition with cationic dye. The effect of pH on the adsorption was illustrated in Fig. 9c. The pH of the solution was increased from pH 3 to 10, the adsorption capacity increased from 68.32 to 99.19 mg/g. In an acidic medium (pH<7), the proton density on the surface sites of rGZ-1:1 composite increased, leading to stronger electrostatic repulsion between the cationic dye and positive charge on the surface and thus resulting in the low adsorption capacity (Li et al., 2011; Fabian et al., 2020). At high pH value (alkaline medium), the electrostatic repulsion decreased, which is due to the surface was negatively charged, resulting in a rise of the cationic dye adsorption capacity. Besides, further increase in range of pH 8 to 10 showed no significant change in adsorption capacity. Thus, from the obtained results indicated that the removal efficiency of MB in range of pH=6-8. In this study, pH 6.2 was chosen according to natural conditions (pH value of MB medium).

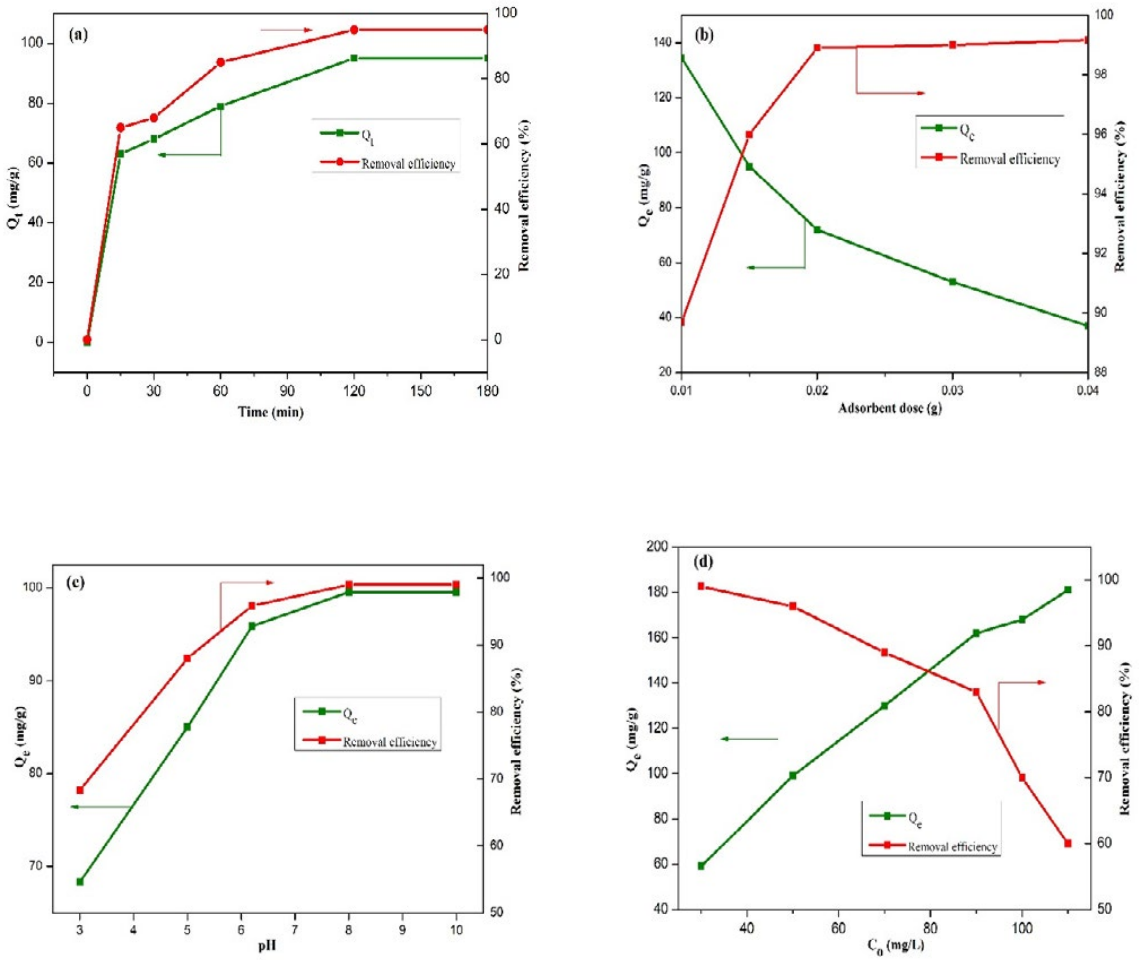

Fig. 9. Effect of different parameters on the adsorption of MB onto rGZ-1:1: (**a**) adsorption time (pH 6.2; adsorbent dosage: 0.015; MB concentration: 50 mg/L; temperature: 30 °C), (**b**) adsorbent dosage (pH 6.2, MB concentration: 50 mg/L; time: 2h; temperature: 30 °C), (**c**) pH (adsorbent dosage: 0.015; MB concentration: 50 mg/L; time: 2 h; temperature: 30 °C) and (**d**) dye concentration (pH 6.2; adsorbent dosage: 0.015; time: 2 h; temperature: 30 °C).

Effect of MB concentration

The MB adsorption with various initial concentration onto the rGZ-1:1 composite was investigated and the results were illustrated in Fig. 9d. When MB concentration increased from 30 to 110 mg/L, the adsorption capacity extended from 59.01 mg/g to 189.39 mg/g, while the adsorption efficiency decreased from 99.01% to 60.39%. This can be explained as follows: the increased MB concentration of MB resulting in the driving force for mass transfer also rises. At low MB concentration, empty sites will appear on the surface of rGZ-1:1 composite, leading to a decrease in adsorption capacity. At high MB concentrations, the active sites required for the dye adsorption are not enough, thus reducing the adsorption efficiency (Luo et al., 2010).

Adsorption isotherm

The adsorption process and the adsorption mechanisms have been widely studied using adsorption isotherm modes. Both isotherm models Langmuir and Freundlich were employed for the analysis of equilibrium adsorption capacity data.

The linear Langmuir equation is expressed as:

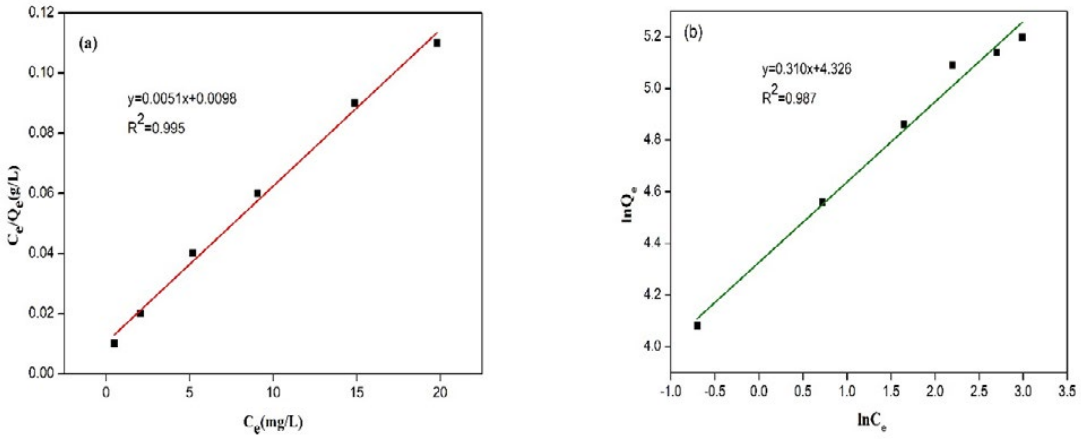

Fig. 10. Langmuir (**a**) and Freundlich (**b**) plots for the MB adsorption onto rGZ-1:1 composite (adsorption conditions: pH 6.2; adsorbent dosage: 0.015 g; adsorption time: 2 h; environment temperature, 30 °C)

$$\frac{C_e}{Q_e} = \frac{C_e}{Q_{\max}} + \frac{1}{Q_{\max} K_L} \tag{4}$$

where, C_e is the MB concentration at equilibrium (mg/L); Q_e and Q_{max} are the MB adsorption capacity at equilibrium and the maximum adsorption capacity of the monolayer coverage (mg/g), respectively; and K_L is constant of Langmuir adsorption equilibrium (L/mg). The values of Q_{max} and K_L were determined based on plotting the C_e/Q_e versus C_e values. An equilibrium parameter, R_L, was used to determine whether the adsorption process is favorable or not and is given by the equation (Luo et al., 2010):

$$R_L = \frac{1}{1 + K_L C_o} \tag{5}$$

where, K_L is constant of Langmuir adsorption equilibrium (L/mg), and C_o is the initial concentration of MB (mg/L). The R_L value shows that the adsorption is favorable when R_L is between 0 and 1, and irreversible when R_L=0 or greater than 1. Fig. 10a showed the Langmuir plot of MB adsorption onto rGZ-1:1 composite. It can be observed from the Langmuir model, the correlation coefficient (R^2) of the isotherms was higher than 0.995, supporting that the adsorption process was quite appropriate for the Langmuir model.

The maximum adsorption Q_{max} of MB dye was 95.87 mg/g at environment temperature (30 °C). This number is higher than previously reported numbers 47.62 mg/g by Pathania group using activated carbon synthesized from Ficus carica bast (Pathania et al. 2017), 17.3 mg/g by Ramesha group using exfoliated graphene oxide materials (Ramesha et al., 2011). It can be concluded that the synthesized composite has an excellent adsorption efficiency of MB dye from aqueous solution. The calculated values R_L were in a range of 0.017 and 0.06 supporting that the adsorption process is favorable.

The linear Freundlich equation is expressed as:

$$logQ_e = logK_F + \frac{1}{n} logC_e \tag{6}$$

where, Q_e is the MB adsorption capacity at equilibrium (mg/g), C_e is the concentration of MB in solution at equilibrium (mg/L), K_F is the Freundlich constant related to adsorption capacity

Table 3. Results of different isotherm plots for the MB adsorption onto rGZ-1:1 composite

Langmuir				Freundlich		
R_L	Q_m (mg/g)	K_L (L/mg)	R^2	K_F (mg/g (mg/L)$^{1/n}$)	1/n	R^2
0.017–0.06	196.08	0.520	0.995	75.641	0.310	0.987

Table 4. Kinetic parameters for MB adsorption onto rGZ-1:1

Pseudo-first-order	R_1^2	k_1 (min^{-1})	$^{*}Q_{e,exp}$ (mg/g)	$^{**}Q_{e,cal}$ (mg/g)
$\ln(Q_e-Q_t) = 4.2036 - 0.0328t$	0.9399	0.0328	96.89	66.93
Pseudo-second-order	R_2^2	k_2 (g/mg min)	$Q_{e,exp}$ (mg/g)	Q_e (mg/g)
$t/Q_t = 0.0097t + 0.1132$	0.9962	8.3×10^{-4}	96.89	103.10

Note: $^{*}Q_{e,exp}$ and $^{**}Q_{e,cal}$ are the experimental adsorption capacity and calculated adsorption capacity (mg/g), respectively.

(mg/g (mg/L)$^{1/n}$). The value of $1/n$ is an experimental parameter and this value is in range of $0.1 < 1/n < 1$, indicating that favorable adsorption process (Luo et al., 2010; Pathania et al. 2017). From Fig. 10b, the Freundlich constant (K_L) was determined and the results were illustrated in Table 3. The correlation coefficient value obtained from Freundlich model was 0.987 and the value of the adsorption intensity $1/n$=0.31 for MB adsorption indicates that the adsorption process fitted to Freundlich model. The value of the correlation coefficient (0.987) was similar to the Langmuir (0.995). Therefore, adsorption of MB dye onto rGZ-1:1 composite fit well with both Langmuir and Freundlich models.

Adsorption kinetics

The kinetics of the MB adsorption process were modeled based on a controlling temperature of 30 °C, 0.015 g of the synthesized rGZ-1:1 composite and a pH 6.2, and the pseudo-first-order kinetic rate is presented as equation (7):

$$\ln(Q_e - Q_t) = \ln Q_e - k_1 t \tag{7}$$

Where, Q_e and Q_t (mg/g) are the MB adsorption capacity at the time of equilibrium and at time t (min); k_1 is the pseudo-first-order rate constant (min^{-1}). As the obtained results from Table 4, the values of k_1 and Q_e were calculated using the ln (Q_e–Q_t) versus time (t) plot indicated that the pseudo-first-order rate was not suitable for MB adsorption process. The value of the correlation coefficient R^2_1 was low (~0.94) was not marked of pseudo-first-order kinetics for the MB dye adsorption.

Conversely, if the adsorption of MB followed pseudo-second-order kinetics, the equation can be presented as follows:

$$\frac{t}{Q_t} = \frac{1}{k_2 Q_e^2} + \frac{1}{Q_e} t \tag{8}$$

Where, k_2 is the pseudo-second-order rate constant (g/mg min), and t is the adsorption time. The values of Q_e and k_2 were determined from the linearity of the t/Q_t versus adsorption time (t) plot (Fig. 11). From the obtained results showed the correlation coefficients R_2^2=0.9962, which suggested that the pseudo-second-order kinetic was more suitable to express the adsorption of MB dye to produced materials.

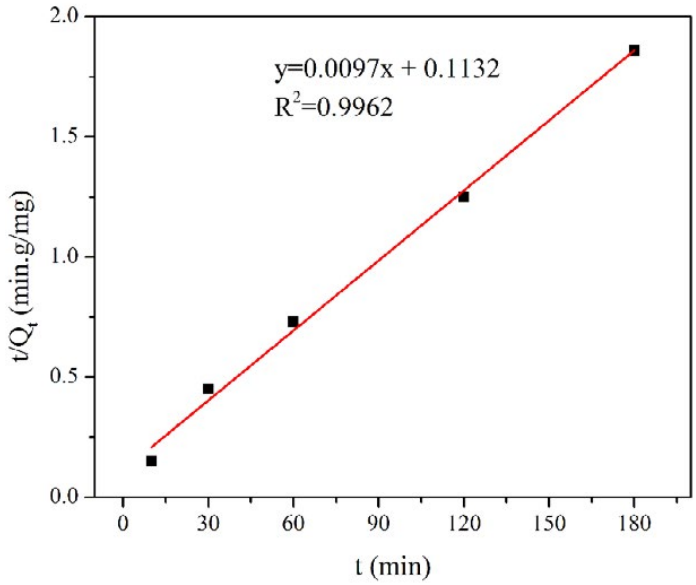

Fig. 11. Pseudo-second-order kinetic graph for MB adsorption onto rGZ-1:1 composite (adsorption conditions: pH 6.2; adsorbent dosage: 0.015 g; dye concentration, 50 mg/L; environment temperature, 30 °C)

CONCLUSIONS

In conclusion, the ZSM-5@rGO composite, with excellent adsorption capacity, was synthesized by one-pot procedure using expanded perlite and rGO as precursors. The as-synthesized materials were characterized by XRD, FT-IR, Raman, SEM and N_2 adsorption-desorption isotherm. The influence of rGO/ZSM-5 ratio on MB adsorption was investigated. The MB adsorption process using ZSM-5@rGO composite was studied according to the batch model and the results showed that the ratio of rGO/ZSM-5=1/1 (by weight) provided the best adsorption efficiency. The study of adsorption isotherm indicated that the adsorption process were well fit with both Langmuir and Freundlich models. The values of R_L and *1/n* acquired from Langmuir and Freundlich models, respectively, demonstrated that the MB adsorption was favorable and the highest monolayer adsorption capacity was up to 95.87 mg/g. The adsorption kinetics study showed that the pseudo-second-order kinetic model was more suitable for the synthesized materials. Based on the above results, the ZSM-5@rGO composite could be used as an economical adsorbent and effectively remove MB dye from sewerage.

GRANT SUPPORT DETAILS

The present research has been financially supported by the Vingroup Joint Stock Company through the Domestic Master/ PhD Scholarship Programme of Vingroup Innovation Foundation (VINIF), Vingroup Big Data Institute (VINBIGDATA), code VINIF.2020.ThS.19.

CONFLICT OF INTEREST

The authors declare that there is not any conflict of interests regarding the publication of this manuscript. In addition, the ethical issues, including plagiarism, informed consent, misconduct, data fabrication and/or falsification, double publication and/or submission, and redundancy has been completely observed by the authors.

LIFE SCIENCE REPORTING

No life science threat was practiced in this research.

REFERENCES

Abalos, R.; Erdmann, E. and Destefanis, H.A. (2003). Surface modifications of volcanic glasses (perlites) by water vapor. Lat. Am. Appl. Res., 33, 59–62.

Bagane, M. and Guiza, S. (2000). Removal of a dye from textile effluents by adsorption. Annales de Chimie-Science des Matériaux, 25, 615–625.

Belova, T.P. (2019). Adsorption of heavy metal ions (Cu^{2+}, Ni^{2+}, Co^{2+} and Fe^{2+}) from aqueous solutions by natural zeolite. Heliyon, 5, e02320.

Cadiam, M.B.; Rajangam, V.; Balachandran, S.; Aziz, A.; Mei, M.P.; Wang, S.C. and Hyun-Tae J. (2016). Characterization of reduced graphene oxide supported mesoporous Fe_2O_3/TiO_2 nanoparticles and adsorption of As (III) and As (V) from potable water. J. Taiwan Inst. Chem. Eng., 62, 199–208.

Chen, L.; Yang, J.; Zeng, X.; Zhang, L. and Yuan, W. (2013). Adsorption of methylene blue in water by reduced graphene oxide: Effect of functional groups. Mater. Express, 3, 281–290.

Chen, N.Y. (1996). Shape selective catalysis in industrial applications, Second Edition. CRC press 65.

Choudhury, P.; Chattopadhyay, S.; De, G. and Basu, B. (2021). Ni–rGO–zeolite nanocomposite: an efficient heterogeneous catalyst for one-pot synthesis of triazoles in water. Mater. Adv., 2, 3042–3050.

Corregidor, P.F.; Acosta, D.E. and Destéfanis, H.A. (2014). Green synthesis of ZSM-5 zeolite prepared by hydrothermal treatment of perlite. Effect of chemical composition and characterization of the product. Sci. Adv. Mater., 6, 1203–1214.

Da Silva Filho, S.H.; Vinaches, P. and Pergher, S.B.C. (2018). Zeolite synthesis in basic media using expanded perlite and its application in Rhodamine B adsorption. Mater. Lett., 227, 258–260.

Dai, M. (1998). Mechanism of adsorption for dyes on activated carbon. J. Colloid. Interface Sci., 198, 6–10.

Fabian, A.A.; Marco, G.; Talia, T.; Paola, A.; Raul, M.; Andrea, V.; Orlando, S.; Cristian, V.G.; Melvin, A. and Lorenzo, S.C. (2020). The adsorption of methylene blue on eco-friendly reduced graphene oxide. Nanomaterials, 10 (4), 681.

Faghihian, H. and Kamali, M. (2003). Synthesis of Na-Pc zeolite from perlite and study of its ability to remove cyanide from liquid wastes. Int. J. Environ. Pollut., 19, 557-566.

Fan, W.; Li, R.; Ma, J.; Fan, B. and Cao, J. (1995). Synthesis, characterization and catalytic properties of MFI-type zeolites prepared in the system $Na_2O–SiO_2–Al_2O_3–H_2N(CH_2)_6NH_2–NH_4F$. Microporous Mater., 4, 301–307.

Feng, P.; Xuchen, L.; Qingshan, Z.; Zhimin, Z.; Yan, Y. and Shiwei. (2015). Direct synthesis of HZSM-5 from natural clay. J. Mater. Chem. A., 3, 4058–4066.

Filho, S.H.S.; Vinaches, P. and Pergher, S.B.C. (2018). Zeolite synthesis in basic media using expanded perlite and its application in Rhodamine B adsorption. Mater. Lett., 227, 258-260.

Gao, W. (2015). The chemistry of graphene oxide. Graphene oxide Springer, 61–95.

Gök. Ö.; Özcan, A.S. and Özcan, A. (2010). Adsorption behavior of a textile dye of Reactive Blue 19 from aqueous solutions onto modified bentonite. Appl. Surf. Sci., 256, 5439–5443.

Hauchhum, L. and Mahanta, P. (2014). Carbon dioxide adsorption on zeolites and activated carbon by pressure swing adsorption in a fixed bed. Int. J. Energy. Environ. Eng., 5, 349–356.

Hernandez, J.M.M.; San German C.M.R.; Arceo, L.D.B.; Villalobos, L.Z. and Flores, M.E. (2013). Synthesis and characterization of carbon nanospheres obtained by microwave radiation. Carbon, 54, 168–174.

Hummers, Jr.W.S and Offeman, R.E. (1958). Preparation of graphitic oxide. J. Am. Chem. Soc., 80, 1339.

Imamura, K.; Ikeda, E.; Nagayasu, T.; Sakiyama, T. and Nakanishi, K. (2002). Adsorption behavior of methylene blue and its congeners on a stainless steel surface. J. Colloid. Interface Sci., 245, 50-70.

Jorge, G.I.; Margarita, H.-E.; Carmen, D.-S.; Arturo, F.-I.; Mono, M.S. (2008). The point of zero charge of oxides. Environ. Chem., 70–78.

Khatamian, M.; Khodakarampoor, N.; Oskoui, M.S. and Kazemian, N. (2015). Synthesis and characterization of RGO/zeolite composites for the removal of arsenic from contaminated water. RSC Adv., 5, 35352–35360.

Khatamian, M.; Khodakarampoor, N. and Saket-Oskoui, M. (2017). Efficient removal of arsenic using graphene-zeolite based composites. J. Colloid. Interface Sci., 498, 433-441.
Kim, D.W.; Han, H.; Kim, H.; Guo, X. and Tsapatsis, M. (2018). Preparation of a graphene oxide/faujasite composite adsorbent. Micropor. Mesopor. Mat., 268, 243–250.
Król, M. (2020). Natural vs. synthetic zeolites. Crystals, 10 (7), 622.
Li, B.; Cao, H. and Yin, G. (2011). $Mg(OH)_2$@reduced graphene oxide composite for removal of dyes from water. J. Mater. Chem., 21, 13765–13768.
Li, D.; Qiu, L.; Wang, K.; Zeng, Y.; Li, D.; Williams, T.; Huang, Y.; Tsapatsis, M.; Wang, H. (2012). Growth of Zeolite Crystals with Graphene Oxide Nanosheets. Chem. Comm., 48 (16), 2249–2251.
Liu, Y.; Lu, H. (2020). Synthesis of ZSM-5 zeolite from fly ash and its adsorption of phenol, quinoline and indole in aqueous solution. Mater. Res. Express, 7, 55506.
Liu, Y.S.; Jiang, X.Q.; Li, B.J.; Zhang, X.D.; Liu, T.Z.; Yan, X.S.; Ding, J.; Cai, Q. and Zhang, J.M. (2014). Halloysite nanotubes@reduced graphene oxide composite for removal of dyes from water and as supercapacitors. J. Mater. Chem. A., 2, 4264-4269.
Luo, P.; Zhao, Y.; Zhang, B.; Liu, J.; Yang, Y. and Liu, J. (2010). Study on the adsorption of Neutral Red from aqueous solution onto halloysite nanotubes. Water Res., 44 (5), 1489-97.
Magdalena, K.; Justyna, M.; Włodzimierz, M. and Waldemar, P. (2014). Low-temperature synthesis of zeolite from perlite waste – Part II: characteristics of the products. Mater. Sci.-Pol., 32, 526 - 532
Mei, X.; Meng, X. and Wu, F. (2015). Hydrothermal method for the production of reduced graphene oxide. Phys. E Low-Dimens. Syst. Nanostruct., 68, 81–86.
Navrotsky, A. (1994). Thermochemistry of crystalline and amorphous silica. Rev. Mineral. Geochem., 29, 309–329.
Pathania, D.; Sharma, S. and Singh, P. (2017). Removal of methylene blue by adsorption onto activated carbon developed from Ficus carica bast. Arab. J. Chem., 10, S1445–S1451.
Prasun, C.; Shreyasi, C.; Goutam, D.; Basudeb, B. (2021). Ni–rGO–zeolite nanocomposite: an efficient heterogeneous catalyst for one-pot synthesis of triazoles in water. Mater. Adv., 2 (9), 3042–3050.
Ramesha, G.K.; Kumara, A.V.; Muralidharam, H.B. and Sampath, S. (2011). Graphene and graphene oxide as effective adsorbents toward anionic and cationic dyes. J. Colloid. Interface Sci., 361, 270–277.
Sismanoglu, T.; Kismir, Y. and Karakus, S. (2010). Single and binary adsorption of reactive dyes from aqueous solutions onto clinoptilolite. J. Hazard. Mater., 184, 164–169.
Sourav, S.; Tapas, K.G.; Dipak, R.; Indranil, R.; Amarty, B.; Gunjan, S.; Mukut, C. and Dipankar, C. (2016). Studies on synthesis of reduced graphene oxide (RGO) via green route and its electrical property. Mater. Res. Bull., 79, 41–51.
Taddeo, R.; Prajapati, S. and Lepistö, R. (2017). Optimizing ammonium adsorption on natural zeolite for wastewaters with high loads of ammonium and solids. J. Porous Mater., 24, 1545–1554.
Tan, T.V.; Vinh, T.L.; Tuan, V.P.; Giang, T.V. (2022). The highly efficient purification capacity of rGO-zeolite composites for aged oil in transformer machines. Arab. J. Chem., 15 (3), 103683.
Uddin, M.T.; Islam, M.A.; Mahmud, S. and Rukanuzzaman, M. (2009). Adsorptive removal of methylene blue by tea waste. J. Hazard. Mater., 164, 53–60.
Vu, T.T.; La, T.V.; Pham, V. T..; Minh Khoi, V.; Huynh, D.C. and Tran, N.K. 2020. Highly Efficient Adsorbent for the Transformer Oil Purification by ZnO/Graphene Composite. Arab. J. Chem., 13 (11), 7798–7808.
Vuong, H.N.T.; Anh, T.N.T.; Van, D.H.V.; Cuong, N.D.; Khieu, D.Q and Vo, V. (2016). Fe_3O_4/reduced graphene oxide nanocomposite: synthesis and its application for toxic metal ion removal. J. Chem., 2016, 10 pages.
Vuong, H.T.N.; Minh, N.N.; Tam, T.T.; Tien, T.N.; Huan, V.D and Xuan, N.P. (2020). One-pot preparation of alumina-modified polysulfone-graphene oxide nanocomposite membrane for separation of emulsion-oil from wastewater. J. Nanomater., 2020, 12 pages.
Wang, Y.; Feng, R.; Li, X.; Liu, X. and Yan, Z. (2013). In situ synthesis, characterization and catalytic activity of ZSM-5 zeolites on kaolin microspheres from amine-free system. J. Porous Mater., 20, 137–141.
Xuan, N.P.; Hoa, T.N.; Nhung, T.P.; Bao, T.T.N.; Manh, B.N.; Thi, V.T.T.; Huan, V.D. (2020). Green synthesis of H-ZSM-5 zeolite-anchored O-doped g-C_3N_4 for photodegradation of Reactive Red 195

(RR 195) under solar light. J. Taiwan Inst. Chem. Eng., 114, 91–102.
Yang, Z.; Ji, S.; Gao, W.; Zhang, C.; Ren, L.; Tjiu, W.W.; Zhang, Z.; Pan, J. and Liu, T. (2013). Magnetic nanomaterial derived from graphene oxide/layered double hydroxide hybrid for efficient removal of methyl orange from aqueous solution. J. Colloid. Interface Sci., 408, 25–32.
Yushan, L.; Xiaoqing, J.; Baojun, L.; Xudong, Z.; Tiezhu L.; Xiaoshe, Y.; Jie, D.; Qiang C. and Jianmin, Z. (2014). Halloysite nanotubes@reduced graphene oxide composite for removal of dyes from water and as supercapacitors. J. Mater. Chem. A., 12, 4264–4269.
Zhang, W.; Wang, K,; Yu, Y. and He, H. (2010). TiO_2/HZSM-5 nano-composite photocatalyst: HCl treatment of NaZSM-5 promotes photocatalytic degradation of methyl orange. Chem. Eng. J., 163, 62–67.